

Incorporating Phase-Dependent Polarizability in Nonadditive Electrostatic Models for Molecular Dynamics Simulations of the Aqueous Liquid–Vapor Interface

Brad A. Bauer, G. Lee Warren, and Sandeep Patel*

Department of Chemistry and Biochemistry, University of Delaware, Newark, Delaware 19716

Received August 5, 2008

Abstract: We discuss a new classical water force field that explicitly accounts for differences in polarizability between liquid and vapor phases. The TIP4P-QDP (4-point transferable intermolecular potential with charge-dependent polarizability) force field is a modification of the original TIP4P-FQ fluctuating charge water force field of Rick et al. [*J. Chem. Phys.* 1994, 101, 6141] that self-consistently adjusts its atomic hardness parameters via a scaling function dependent on the *M*-site charge. The electronegativity (χ) parameters are also scaled in order to reproduce condensed-phase dipole moments of comparable magnitude to TIP4P-FQ. TIP4P-QDP is parametrized to reproduce experimental gas-phase and select condensed-phase properties. The TIP4P-QDP water model possesses a gas phase polarizability of 1.40 Å³ and gas-phase dipole moment of 1.85 Debye, in excellent agreement with experiment and high-level ab initio predictions. The liquid density of TIP4P-QDP is 0.9954 (\pm 0.0002) g/cm³ at 298 K and 1 atm, and the enthalpy of vaporization is 10.55 (\pm 0.12) kcal/mol. Other condensed-phase properties such as the isobaric heat capacity, isothermal compressibility, and diffusion constant are also calculated within reasonable accuracy of experiment and consistent with predictions of other current state-of-the-art water force fields. The average molecular dipole moment of TIP4P-QDP in the condensed phase is 2.641 (\pm 0.001) Debye, approximately 0.02 Debye higher than TIP4P-FQ and within the range of values currently surmised for the bulk liquid. The dielectric constant, ϵ = 85.8 \pm 1.0, is 10% higher than experiment. This is reasoned to be due to the increase in the condensed phase dipole moment over TIP4P-FQ, which estimates ϵ remarkably well. Radial distribution functions for TIP4P-QDP and TIP4P-FQ show similar features, with TIP4P-QDP showing slightly reduced peak heights and subtle shifts toward larger distance interactions. Since the greatest effects of the phase-dependent polarizability are anticipated in regions with both liquid and vapor character, interfacial simulations of TIP4P-QDP were performed and compared to TIP4P-FQ, a static polarizability analog. Despite similar features in density profiles such as the position of the GDS and interfacial width, enhanced dipole moments are observed for the TIP4P-QDP interface and onset of the vapor phase. Water orientational profiles show an increased preference (over TIP4P-FQ) in the orientation of the permanent dipole vector of the molecule within the interface; an enhanced *z*-induced dipole moment directly results from this preference. Hydrogen bond formation is lower, on average, in the bulk for TIP4P-QDP than TIP4P-FQ. However, the average number of hydrogen bonds formed by TIP4P-QDP in the interface exceeds that of TIP4P-FQ and observed hydrogen bond networks extend further into the gaseous region. The TIP4P-QDP interfacial potential, calculated to be −11.98 (\pm 0.08) kcal/mol, is less favorable than that for TIP4P-FQ by approximately 2% as a result of a diminished quadrupole contribution. Surface tension is calculated within a 1.3% reduction from the experimental value. Results reported demonstrate TIP4P-QDP as a model comparable to the popular TIP4P-FQ while accounting for a physical effect neglected by many other classical water models. Further refinements to this model, as well as future applications are discussed.

I. Introduction

The study of liquid–vapor interfacial systems has enjoyed a rich history of experimental and theoretical investigation.^{2–11} Recent advances in experimental methodologies and protocols^{12–14} including sum frequency generation (SFG) and second

harmonic generation (SHG) spectroscopies as well as improvements in computational modeling^{15,16} continue to elucidate atomically resolved structural, dynamical, and thermodynamic aspects of such systems. Aqueous solution–vapor interfaces, in particular, have generated intense interest due to the importance of such systems in atmospheric, environmental, and biological chemistry.^{15–17}

* Corresponding author. E-mail: sapatel@udel.edu.

Computational approaches to the atomistic modeling of liquid–vapor interfaces, such as molecular dynamics and Monte Carlo techniques, have become viable in recent decades due to advances in computational hardware and improvements in simulation algorithms. Such techniques employ simplified empirical interaction models, or force fields, which are classical models parametrized to properties derived from experiment or first principles calculations on carefully selected training systems.¹⁸ In these models, the electrostatic contribution to the intermolecular interaction potential is described by a Coulombic interaction between molecular charge distributions which are constructed from fixed atomic partial charges or multipole moments placed throughout each molecule.^{19–21} Unfortunately, fixed-moment representations of these classical interaction models also entail a number of shortcomings^{22–25} which limit overall simulation accuracy. In particular, nonadditive polarization and induction effects are ignored and there is no explicit provision for describing charge transfer effects. Consequently, community interest in polarizable force fields is growing and the development of polarizable models for inorganic ions,^{26–31} small molecules,^{1,24,26,32–39} and larger biologically relevant macromolecules^{40–50} is rapidly increasing in pace even though such models have not yet realized the popularity enjoyed by fixed-charge models. This heightened interest has fostered several different approaches for modeling atomic and molecular polarization including point-dipole (and higher-order multipole) polarizable models,^{35,51,52} Drude oscillator models,^{30,36,37,53–55} and charge equilibration/fluctuating charge models.^{1,24,38,39,41,42,48,56–68}

Polarizable interaction models that incorporate dipole induction effects have already proven to be an indispensable tool for obtaining an accurate theoretical estimation of solution structure and thermodynamics in interfacial systems such as aqueous solutions of inorganic salts.^{27,32,34,69–73} The success of such models stems from a dipole induction response that is sensitive to the local electrostatic environment. However, one particular aspect of such models that has not received specific attention is the variation of *molecular polarizability* with phase which recent theoretical investigations have demonstrated is decreased in the condensed phase environment relative to the gas phase. Instead, many current polarizable force fields parametrized specifically for condensed phase environments employ a fixed molecular polarizability which is reduced in magnitude relative to the gas phase value in order to achieve stable dynamics and acceptable condensed-phase properties.^{34,36,37,53,64,66,74} While such an approach is perhaps adequate in an isotropic bulk environment, a description based on a fixed, scaled molecular polarizability can be questioned in the presence of anisotropic environments such as the aqueous liquid–vapor interface where the bulk environment transitions to the vacuum over molecular length scales. Indeed, some dipole polarizable models such as the AMOEBA model⁷³ which employ gas phase polarizabilities also incorporate Thole-type damping at short-range to prevent unstable overpolarization in the condensed phase.

Currently, there are few models that are able to explicitly account for this effect within the context of a molecular dynamics or Monte Carlo simulation and, to our knowledge, none that explicitly consider a dynamically responsive

molecular polarizability. Consequently, our objective in the present work is to present a water force field that effectively allows for the variation of molecular polarizability with phase; more specifically, as will be discussed, molecular polarizability is coupled to variable atomic partial charges which, for the specific aim of modeling the neat water liquid–vapor interface, offers a simple and continuous phase-dependent parameter to which polarizabilities may be coupled.

Section II presents the development of trends necessary for establishing the charge dependent polarizable (TIP4P-QDP) water model (II.A), implications of applied scaling based on these trends within the charge equilibration formalism (II.B), and the details of the condensed phase and liquid–vapor interfacial simulations (II.C). Section III presents the parametrization of this model (III.A), results of the condensed phase (III.B), and liquid–vapor interfacial (III.C) simulations and offers a comparison of the TIP4P-QDP (4-point transferable intermolecular potential with charge-dependent polarizability) model to the original TIP4P-FQ model. We conclude our study with a general discussion and perspectives on future work in Section IV.

II. Theoretical Methods and Force Fields

A. Phase-Dependent Polarizabilities. A variety of recent theoretical investigations involving *ab initio* calculations with polarizable continuum solvent, the partitioning of cluster polarizabilities, and the temperature/density dependence of dielectric constants of fluids reasonably establish that the surrounding condensed phase environment can significantly affect the polarizability of a solvated molecule. Krishtal et al. have previously reported that the average intrinsic polarizability of water molecules decreases as the size of a cluster increases and also as the number and types of hydrogen bonds on a molecule increases.⁷⁵ The notion of decreasing polarizability in condensed regions is further supported by the *ab initio* calculations of Morita involving water clusters⁷⁴ which suggest that the condensed-phase polarizability of water should be 7–9% lower than that of the gas phase value. The spatial constraints imposed by condensed-phase environments limit the number of accessible excited states and diffuse character of the electron density distribution as dictated by Pauli's exclusion principle.^{30,74} A recent study by Schropp and Tavan⁷⁶ further suggests that the average effect of the inhomogeneous electric fields *within* the molecular volume of a single water molecule are consistent with classical parametrizations of polarizable water force fields in which the molecular polarizability is assigned a value around 68% of the gas-phase value.

While these results indicate a reduction of polarizability within the condensed phase, the implications for the rate and nature of the decrease remain unclear. Similarly, a self-consistent analytic formalism capable of correlating changes in molecular polarizability to atomic or molecular properties remains undetermined. While it has been observed that metrics such as aggregation number, hydrogen bonding, or local density are associated with a phase-dependent decrease in molecular polarizability, such metrics are impractical from

the perspective of a molecular dynamics simulation. Consequently, a relationship between the polarizability and an atomic property that smoothly and monotonically transitions from one phase to another is desirable in attempting to establish a simple functional form for polarizability change between phases.

One potentially useful parameter for modeling phase-dependent changes in polarizability is the dipole moment of the molecule. Both experiment and theoretical calculations such as *ab initio* molecular dynamics simulations demonstrate a difference in molecular dipole moments between the condensed phase and gas phase environments.^{16,77,78} Although there is no consensus on an exact value of the average condensed-phase dipole moment of water, it is accepted that the average dipole moment increases upon condensation. Since dipole moments within classical molecular dynamics simulations are readily obtained from the atomic positions and partial charges, no additional information based on neighboring molecules is explicitly required. If a rigid water geometry is chosen, the calculation is even further simplified in that the dipole moment may be determined solely from the magnitude of the associated atomic partial charges.

Within the charge equilibration/fluctuating charge formalism, atomic hardnesses determine molecular polarizability. Thus, a plausible approach to modeling a phase-dependent polarizability in water lies in coupling the atomic charges to the atomic hardness parameters. A similar approach has been previously implemented by Rappé and Goddard for the hydrogen atom in which a linear charge dependence is introduced into the corresponding atomic hardness value.⁵⁸ Most generally, each atomic hardness function will depend simultaneously on all partial charges within the molecule; however, this introduces an unnecessary level of complexity into the model. A more simplistic approach entails modulating or scaling all of the atomic hardness values within a molecule based on a single parameter based on the polarization state of the molecule. This parameter may be chosen to be an instantaneous function of all atomic charges within the molecule (such as the dipole moment). However, for water, the average molecular dipole moment appears to be correlated with an increased negative partial charge on the oxygen atom. Consequently, the model may be significantly simplified by coupling the atomic hardnesses directly to the oxygen partial charge.

B. Charge-Dependent Polarizable Model. The charge equilibration formalism, based on Sanderson's idea of electronegativity equalization,⁷⁹ offers one convenient route to incorporating a local chemical environmental dependence of the molecular polarizability. Polarization of the electronic density (modeled classically as a distribution of atomic partial charges) is affected by the redistribution of charge density within the molecule in an effort to equalize the instantaneous electrostatic chemical potential in the presence of external electric fields arising from nearby molecules. The directionality and ease of charge redistribution is determined by parametrized physical properties of individual atoms. Further details regarding the specifics of charge equilibration methods are available in the literature.^{1,24,39,48,58–60,68,79–82}

The charge equilibration electrostatic energy of an N -atom molecule in the absence of an external electric field, each atom carrying partial charge Q_i , is

$$E(Q) = \sum_{i=1}^N \left(\chi_i Q_i + \frac{1}{2} \eta_i Q_i^2 \right) + \sum_{i<j}^N Q_i Q_j J_{ij} + \lambda \left(\sum_{i=1}^N Q_i - Q_{\text{total}} \right) \quad (1)$$

where the χ_i 's are atom electronegativities and the η_i 's are atomic hardnesses. The J_{ij} terms represent the interatomic hardness terms for each pair of atoms i and j within a molecule. A standard Coulomb interaction is employed between each pair of atoms located on different molecules. The last term in eq 1 describes a molecular charge constraint applied to the entire molecule and enforced via the Lagrange multiplier λ . In the following, we will specifically focus on a TIP4P-FQ water molecular geometry which consists of three charge carrying sites: two hydrogen sites and one off-atom M -site located along the angle bisector.

In order to establish an appropriate correspondence between charge and polarizability, we consider the polarizability expression for a TIP4P-FQ molecule within the charge equilibration formalism:^{83,84}

$$\alpha = \mathbf{R}^T \mathbf{J}^{-1} \mathbf{R} \quad (2)$$

where α is the 3×3 polarizability tensor, and \mathbf{R} is the 3×4 position matrix. \mathbf{J} is the 4×4 hardness matrix comprised of the diagonal η terms and the off-diagonal J -terms and augmented by a molecular charge neutrality constraint as

$$\mathbf{J} = \begin{pmatrix} \eta_M & J_{MH} & J_{MH} & 1 \\ J_{MH} & \eta_H & J_{HH} & 1 \\ J_{MH} & J_{HH} & \eta_H & 1 \\ 1 & 1 & 1 & 0 \end{pmatrix} \quad (3)$$

Similarly, the position matrix is also augmented to ensure proper dimensions for matrix operations. Equations 2 and 3 illustrate that the polarizability may be directly related to the molecular geometry and inverse atomic hardnesses. For a rigid molecule such as TIP4P-FQ where the position matrix \mathbf{R} is fixed, a charge-dependent polarizability may be obtained by introducing an explicit charge dependence into the corresponding hardness matrix elements. Most generally, we modify both the hardness and electronegativity parameters as a function of charge to incorporate the desired phase-dependent polarizable effect:

$$E(Q) = \sum_{i=1}^N \chi_i(Q_M) Q_i + \frac{1}{2} \sum_{i=1}^N \eta_i(Q_M) Q_i^2 + \sum_{i<j}^N J_{ij}(Q_M) Q_i Q_j + \lambda \left(\sum_{i=1}^N Q_i - Q_{\text{total}} \right) \quad (4)$$

These modifications are also accounted for in the corresponding energy derivatives (Appendix).

Since the molecular polarizability response is determined by the atomic hardnesses, this suggests that one may readily modulate the effect by applying an appropriate charge-dependent scaling function, $g(Q_M)$, to the atomic hardnesses to yield the following definition for charge-dependent hardness:

$$\mathbf{J}(Q_M) = g(Q_M)\mathbf{J} \quad (5)$$

In order to maintain proper gas- and condensed-phase charge distributions, it is also necessary to scale the electronegativity values in addition to the hardnesses. While reasonable results may be obtained by employing the same scaling factor for both the electronegativities and the hardnesses, finer control of the condensed phase dipole moment distribution is afforded by a tunable factor for the electronegativity scaling. Such flexibility also permits better control of the bulk dielectric constant which may be obtained from the fluctuations of the condensed phase dipole moment.⁸⁵ Empirically, we have chosen to introduce the χ -scaling

$$\chi(Q_M) = \frac{g(Q_M)}{h(Q_M)}\chi = [(1-p) + pg(Q_M)]\chi \quad (6)$$

where p is an empirical parameter that controls the extent to which χ is scaled relative to the hardness scaling function. For $p = 1$, the scaling on electronegativity values is equivalent to that in the hardnesses; similarly, a value of $p = 0$ would correspond to no scaling (i.e., a constant electronegativity with no charge-dependent scaling).

Unfortunately, the explicit introduction of a charge dependence into the molecular hardness matrix has introduced the additional complication that the polarizability expression in eq 2 is no longer exact. Consequently, the corresponding system of equations for the equilibrium charges (and polarizabilities) is now a nonlinear system and must be solved by an iterative approach. In situations where the equilibrium charge distribution is not strongly perturbed by the implicit charge dependence, a slightly modified version of eq 2

$$\alpha_{\beta\gamma}(Q_M) \approx \frac{\alpha_{\beta\gamma}}{\xi(Q_M)} - \left(\frac{\nabla_M g(Q_M) \langle R_\beta | \mathbf{J}^{-1}(r) | \hat{\mathbf{M}} \rangle}{|g(Q_M)|^2 h(Q_M)} \right) \times \left[p\chi_M \langle R_\beta | \mathbf{J}^{-1}(r) | \hat{\mathbf{M}} \rangle + \frac{1}{2}\mu_\gamma \right] \quad (7)$$

(derived in the Appendix) is convenient for obtaining a leading-order approximation of the polarizability in the absence of a fully nonlinear treatment. In the above expression, $\alpha_{\beta\gamma}$ is the $\beta\gamma$ -element of the gas-phase molecular polarizability tensor, $\nabla_M g(Q_M)$ is the derivative of the scaling function with respect to Q_M , R_β is the β -position vector, $\hat{\mathbf{M}}$ is a matrix that selects elements associated with the M -site (since we have chosen our hardness elements to only depend on the M -site charge), and μ_γ is the γ -component of the dipole moment. We see the charge-dependent polarizability differs from the unscaled (gas-phase) value by a multiplicative factor $\xi(Q_M) = g(Q_M)h(Q_M)$ and additive terms, which are related to the M -site hardness and dipole moment, respectively. These additive terms of equal magnitude and opposite sign are small compared to the first term and do not greatly influence $\alpha(Q_M)$ (see Figure 8). If we neglect the additive terms and consider the limit in which $p = 1$, eq 7 reduces to

$$\alpha_{\beta\gamma}(Q_M) \approx \frac{\alpha_{\beta\gamma}}{g(Q_M)} \quad (8)$$

from which it is clearly seen that $\alpha(Q_M)$ modulates the gas-phase polarizability via an inverse relationship with the scaling function, $g(Q_M)$. While eq 8 is effective for illustrative purposes, we have employed eq 7 for calculations of the condensed-phase polarizability within this work.

Having now introduced an explicit charge-dependent polarizability via a simple scaling function $g(Q_M)$, it is relevant to discuss the nature and form of this scaling function. While there is no formal theory connecting charge and polarizability, general trends provide guiding insight. In prior work, Rappé and Goddard have employed atomic hardnesses which depend linearly on charge.⁵⁸ In the context of molecular dynamics simulations, such an approach would necessitate some degree of charge bounding to prevent unfavorable overpolarization or underpolarization and to establish consistent polarizabilities in the gaseous and condensed phases. In light of this we have chosen to employ an error function form which applies constant scaling in the purely condensed-phase and gaseous regions and approximately linear scaling in the intermediate region. The use of the error function is also preferred as it allows smooth transitions between each region, which is necessary to avoid discontinuities in the forces. Thus, we choose an error function of the form

$$g(Q_M) = a - b \operatorname{erf}(c(d - Q_M)) \quad (9)$$

as the scaling function since it incorporates additional empirical parameters which can be utilized to model the desired relationship between polarizability and charge. Parameters a and b collectively define the polarizability at the gaseous and condensed-phase limits. The rate of polarizability change with charge for nonisolated molecules is controlled by c . Collectively, c and d describe the onset of scaling and the range of charges over which polarizability changes. The selection of these parameters and comments regarding the parametrization of this model are discussed further in section III.A.

C. Molecular Dynamics Simulations. Condensed phase simulations of the TIP4P-QDP model are conducted at constant pressure and temperature ($T = 298$ K) using CHARMM.^{86,87} For comparative purposes, analogous simulations of TIP4P-FQ under matching conditions are also performed. 216 molecules of each model are included in their respective simulations. Simulations 25 ns in length are performed for the TIP4P-QDP and TIP4P-FQ models. Conditionally convergent long-range interactions are accounted for using particle mesh Ewald⁸⁸ with $\kappa = 0.37$ and 20 grid points in each dimension (FFT grid spacing). Fictitious charge degrees of freedom are assigned masses of 0.000 069 kcal/(mol \cdot ps²). The Nose–Hoover⁸⁹ method is implemented to couple the charge degrees of freedom to a thermostat at 1 K; this thermostat has a mass of 0.005 kcal/(mol \cdot ps²). A 0.5-fs time step is used for propagating the classical equations of motion using a Verlet leapfrog integrator.

Liquid–vapor interface simulations are performed for 1024 molecules at constant volume and constant temperature ($T = 298$ K). The dimensions used for the box are 24.0 \times 24.0 \times 130.0 Å. Particle mesh Ewald parameters are modified

Table 1. Summary of Simulation Parameters

parameter	condensed-phase	liquid–vapor interface
T (K)	298.	298.
N (molecules)	216.	1024.
simulation length (ns)	25.	30.
time step (fs)	0.5	0.5
QMAS kcal/(mol·ps ²)	0.000069	0.000069
TMAS kcal/(mol·ps ²)	0.005	0.005
κ	0.37	0.33
grid points (1 Å spacing)	20 × 20 × 20	30 × 30 × 120

Table 2. Parameters Used for the Scaling Functions of the TIP4P-QDP model^a

parameter	TIP4P-QDP	QDP-P1
a	1.18022	1.18022
b	0.17985	0.17985
c	−2.33071	−2.33071
d	−1.49180	−1.49180
p	0.80000	1.00000

^a Parameters a – d are coefficients used in the error function (eq 9), and p is the additional scaling factor applied to the scaling of χ (eq 6).

from the condensed phase simulation, with 30 grid points in the transverse directions, 120 grid points in the longitudinal direction, and $\kappa = 0.33$. Simulation lengths of 30 and 75 ns are used for the two models. All other simulation parameters are equivalent to those listed for the condensed phase simulations in Table 1.

III. Results

A. Parameterization of TIP4P-QDP Model. The TIP4P-QDP model is based on the application of the charge-dependent scaling function to the original TIP4P-FQ model; therefore, we retain the TIP4P-FQ geometry in the TIP4P-QDP model. To construct the TIP4P-QDP model, we first modify the TIP4P-FQ hardness values which were originally chosen to mimic a reasonable condensed-phase polarizability for stable bulk simulations; thus, the TIP4P-FQ model has a static polarizability that does not correspond to any theoretical or experimental gas phase value. Since it is desired to establish a polarizability gradient between the gaseous and condensed phases and since the gas-phase polarizability is well-known experimentally, we reparameterize the hardness values to reproduce a reasonable gas-phase polarizability of 1.40 Å³. We note that the resulting TIP4P-QDP gas-phase hardnesses maintain approximately the same relative magnitudes as the original TIP4P-FQ hardnesses. The error function form (eq 9) is then parametrized with the caveat that the gas phase polarizability remains unchanged. In the condensed phase, the hardnesses are scaled by a value of $g(Q_M) > 1$ for charges greater than the equilibrium gas phase charges. The parameters of the scaling function which influence the height, slope, and inflection are determined empirically such that the resulting polarizability distribution is centered about an anticipated condensed phase polarizability 7–9% less than the gas phase value (Table 2). A broad polarizability distribution allows for a description of a greater range of local chemical environments.

Table 3. Comparison of Potential Parameters for the TIP4P-QDP and TIP4P-FQ Models

parameter	TIP4P-FQ ^a	TIP4P-QDP	QDP-P1
ϵ (kcal/mol)	0.28620	0.29012	0.350120
F_{\min} (Å)	3.54586	3.55	3.5646
θ (deg)	104.52	104.52	104.52
r_{OH} (Å)	0.9572	0.9572	0.9572
r_{OM} (Å)	0.15	0.15	0.15
$\chi_M - \chi_H$ (kcal/(mol·e))	68.49	60.63	59.91
J_{MM} (kcal/(mol·e ²))	371.6	309.92	309.92
J_{HH} (kcal/(mol·e ²))	353.0	295.36	295.36
$J_{MH}(r_{MH})$ (kcal/(mol·e ²))	286.4	239.47	239.47
$J_{HH}(r_{HH})$ (kcal/(mol·e ²))	203.6	181.91	181.91

^a Reference 1.

Table 4. Gas-Phase Properties from TIP4P-FQ, TIP4P-QDP, and Experiment

property	TIP4P-FQ ^a	TIP4P-QDP	QDP-P1	experiment
μ (Debye)	1.85	1.85	1.85	1.85 ^b
$\bar{\alpha}$ (Å ³)	1.12	1.40	1.40	1.47 ^c
E_{dimer} (kcal/mol)	−4.50	−4.67	−4.44	−5.4 ± 0.7 ^d
dimer O–O length (Å)	2.92	2.91	2.98	2.98 ^d

^a Reference 1. ^b Reference 113. ^c Reference 114. ^d Reference 115.

Regarding electronegativity scaling, a final value of the p -parameter is determined to be $p = 0.80$; this value generates a condensed phase dipole moment distribution with an average of 2.641 (± 0.001) Debye, similar to that exhibited by the TIP4P-FQ model. Introduction of the scaling function and modification of the hardnesses further necessitated slight reparameterization of the remaining electrostatic and nonbonded parameters. The electronegativities were then reparameterized such that a single water molecule in vacuum minimizes to the experimental dipole moment of 1.85 D. Since the polarizability of TIP4P-QDP in the condensed phase is higher than that of TIP4P-FQ, the Lennard-Jones parameters required minor modification to prevent overpolarization while still reproducing reasonable densities and energetics. The Lennard-Jones parameters were parametrized based on fitting to gas-phase water dimer binding energies and geometries (bond distances). A comparison of the electrostatic and nonbonded parameters for TIP4P-QDP and TIP4P-FQ is presented in Table 3, while the gas phase properties for these two models are compared in Table 4.

For further comparisons, a model consisting of full scaling $p = 1.0$ was also developed and parametrized. The results of this model (hereafter referred to as QDP-P1) are also included in this work as a reference in order to more fully clarify differences between the TIP4P-FQ and TIP4P-QDP models. We point out that the best parametrization of QDP-P1 featured comparable density and polarizability to TIP4P-QDP, but had notably higher dipole moments in the condensed phase ($\langle\mu\rangle \approx 2.75$), an anticipated consequence of scaling electronegativity and hardness equivalently. As will be discussed, the enhanced dipole moments are responsible for increased intermolecular cohesion which ultimately reduced the quality of the QDP-P1 parametrization and necessitated additional scaling of the atomic electronegativities.

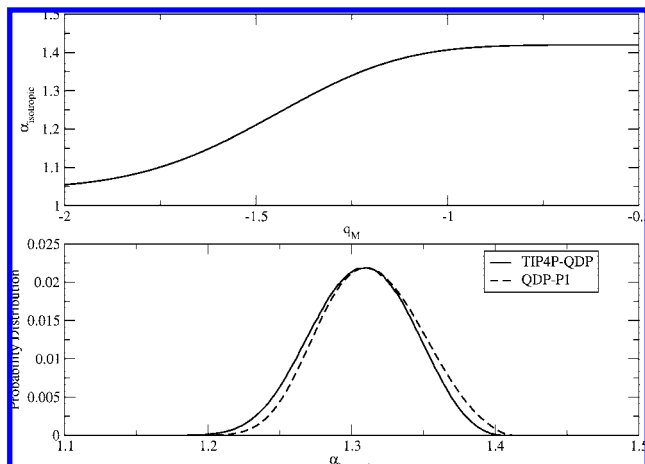


Figure 1. (a) Molecular polarizability (\AA^3) as a function of Q_M . (b) Distribution of molecular polarizabilities within the condensed phase. Polarizabilities were calculated using eq 7 and the charges from simulation.

B. Condensed-Phase Properties. 1. Density. The density of the condensed phase was determined via the expression

$$\rho = \frac{NW}{N_A \langle V \rangle} \quad (10)$$

where N is the number of molecules in the simulation, $\langle V \rangle$ is the average volume of the simulation cell, W is the molecular mass of water, and N_A is Avogadro's number. The average density at 298 K was calculated to be $0.9954 (\pm 0.0002) \text{ g/cm}^3$ for the TIP4P-QDP model. This value is in agreement with the experimental value 0.997 g/cm^3 and reflects the general quality of widely used water models.^{1,54,90–94} As discussed below, the parametrization of the Lennard-Jones parameters to give this density for TIP4P-QDP was balanced with the need to accurately reproduce ΔH_{vap} .

2. Condensed-Phase Polarizability. Since the TIP4P-QDP model adjusts the molecular polarizability dynamically in response to the (electro)chemical environment, we consider the distribution of molecular polarizabilities in the condensed phase. As previously discussed within the context of formulating this model, an isolated TIP4P-QDP molecule was parametrized to a polarizability of 1.40 \AA^3 , a value comparable to the experimental gas phase polarizability. The scaling function allows for TIP4P-QDP molecules to have polarizabilities as low as 1.05 \AA^3 . The polarizability distribution observed in the condensed phase is presented in (Figure 1). M -site charges for every molecule from each snapshot of a trajectory were used in conjunction with eq 7 to generate the polarizability distribution. The average polarizability in the condensed phase is calculated to be $1.309 (\pm 0.001) \text{ \AA}^3$, approximately 17% higher than the static condensed phase polarizability of TIP4P-FQ and about 11% less than the experimental gas phase value. The average condensed-phase value approximately reflects a 6.5% reduction in the molecular polarizability relative to the TIP4P-QDP gas phase value, which agrees well with the estimated range of 7–9% reduction calculated by Morita from first principles.⁷⁴ The distribution also exhibits a width of observed molecular polarizabilities of about 0.20 \AA^3 , which is consistent with the width of the distribution for QDP-P1.

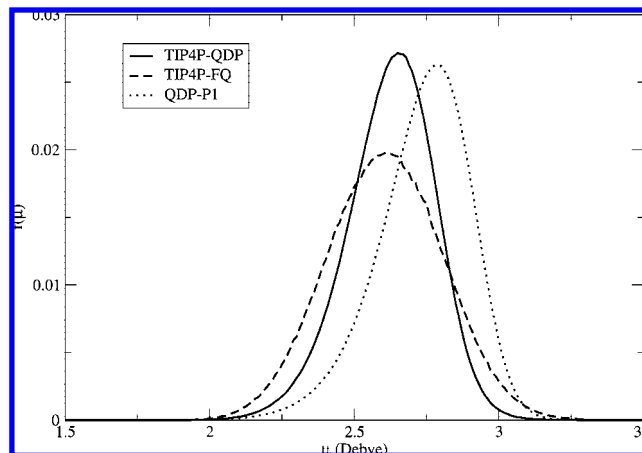


Figure 2. Dipole moment distributions for TIP4P-QDP, TIP4P-FQ, and QDP-P1.

3. Dipole Moment Distribution. The dipole moment distributions for both the TIP4P-QDP and TIP4P-FQ models are presented in Figure 2. The distribution for TIP4P-QDP has an average value of $2.641 (\pm 0.001)$ Debye, almost indistinguishable from that of TIP4P-FQ. While refinement of the p -value could improve the agreement with TIP4P-FQ, such a refinement would be arbitrary due to the uncertainty in the *true* value of the average condensed-phase dipole moment for water. Experimental estimates⁷⁸ of the dipole moment of condensed-phase water ($2.96 \pm 0.6 \text{ D}$) span a broad range of values; this range is also observed in ab initio molecular dynamics simulations.^{16,77} The TIP4P-QDP distribution also features skewed symmetry, with the population of molecules higher dipole moment more sharply declining than those with lower dipole moments. TIP4P-QDP also features a somewhat more narrow distribution than TIP4P-FQ. Although it might seem reasonable that adjustment of the p -value could result in a wider distribution for TIP4P-QDP, various p -values in the range considered during parametrization show essentially the same shape and width, as evident by comparison of the TIP4P-QDP and QDP-P1 distributions. Ab initio studies of bulk water dipole moments demonstrate the importance of local environment, particularly the hydrogen bond coordination, on a molecule's dipole moment.^{95,96} Furthermore, as a molecule becomes more coordinated with hydrogen bonds, the range of accessible dipole moments increases due to an increase in possible structural variations. It is therefore argued that systems with a larger fraction of highly coordinated water molecules will feature wider dipole moment distributions. As is noted in section III.C.3, the average number of hydrogen bonds in the condensed phase is lower for TIP4P-QDP than TIP4P-FQ. In particular, the ratio of water molecules with four hydrogen bonds to molecules with three hydrogen bonds is lower in TIP4P-QDP than TIP4P-FQ (1.4 to 1.8, respectively). Such a change in hydrogen bonding can be reasoned to impact condensed phase properties (such as the higher diffusion constant observed for TIP4P-QDP) and the narrowed dipole moment distribution. We also note that the ratio of hydrogen bonds is consistent between QDP models, further supporting the link between hydrogen bond coordination and dipole moment distribution width. The slight skewed

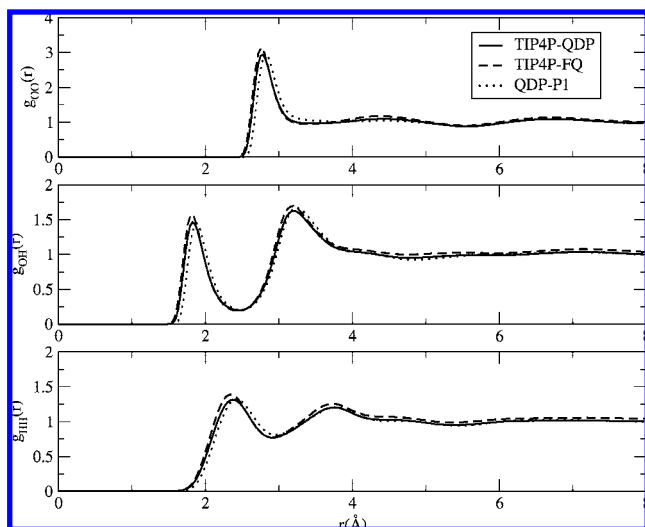


Figure 3. Radial distribution functions for TIP4P-QDP, TIP4P-FQ, and QDP-P1.

character of the TIP4P-QDP dipole moment distribution can be attributed, at least in part, to the selective attenuation of the largest oxygen partial charges due to the significant scaling of the hardnesses in the condensed phase.

4. Radial Distribution Function. Radial distribution functions for TIP4P-QDP and TIP4P-FQ are presented in Figure 3. Although the distributions share similar features, there are subtle differences between the two models. There is a slight reduction in peak height and structure for the TIP4P-QDP model compared to TIP4P-FQ. This feature which is common to the three distributions presented corresponds to a decrease in four-coordinate hydrogen bond formation. This notion of decreased hydrogen bond formation is further discussed below. A subtle shift of the TIP4P-QDP distributions toward larger separation distances is also observed in each distribution. Although this is a rather minor difference from the TIP4P-FQ model, the shift is in better agreement with neutron diffraction data^{97,98} which also features peaks centered at greater distances than predicted by TIP4P-FQ.

5. Enthalpy of Vaporization. Enthalpy of vaporization is defined as

$$\Delta H_{\text{vap}} = \Delta E_{\text{vap}} + \Delta(PV)_{\text{vap}} \quad (11)$$

Noting that the state change in vaporization is from the liquid phase to the vapor phase allows for the expansion to liquid and vapor terms. Making the assumption that the change in volume of the liquid is negligible compared to that of the gas and assuming ideality in the gas phase results in the final expression:

$$\Delta H_{\text{vap}} = E_{\text{gas}} - E_{\text{liq}} + RT \quad (12)$$

Here, the E_{gas} is the energy of a single minimized molecule in vacuum and E_{liq} is the average system energy from condensed-phase simulations. The original TIP4P-FQ model was parametrized to exhibit excellent agreement with the experimental enthalpy of vaporization. The current parametrization of TIP4P-QDP predicts a vaporization enthalpy of $10.55 (\pm 0.12)$ kcal/mol. Although higher than the experiment (10.51 kcal/mol) and TIP4P-FQ (10.49 kcal/mol)

values, the TIP4P-QDP result still agrees well with these two values, exhibiting a 0.4% increase over the experimental value. Additionally, further improvement of this value via modification of the Lennard-Jones parameters appears to have adverse effects on the density of the condensed phase. Thus, in order to ensure reasonable accuracy in both properties, a slight compromise in the model's enthalpy of vaporization was deemed acceptable.

6. Dielectric Constant. The dielectric constant for each system was calculated using the relation:

$$\epsilon = \epsilon_{\infty} + \frac{4\pi}{3k_B T \langle V \rangle} (\langle M^2 \rangle - \langle \mathbf{M} \rangle \cdot \langle \mathbf{M} \rangle) \quad (13)$$

where \mathbf{M} is the dipole moment of the simulation cell. The term ϵ_{∞} is the infinite frequency (optical) dielectric constant, estimated using the approach outlined in ref 54. To summarize, charge dynamics simulations were performed on static configurations generated from an *NVT* simulation at the average density of QDP predicted from constant pressure simulations. The charge degrees are propagated at 1 K, and the Kirkwood fluctuation formula is applied to determine the optical dielectric:

$$\epsilon_{\infty} = 1 + \frac{4\pi}{3k_B T \langle V \rangle} (\langle M^2 \rangle - \langle \mathbf{M} \rangle \cdot \langle \mathbf{M} \rangle) \quad (14)$$

We obtain a dielectric constant of $85.8 (\pm 1.0)$ where the contribution from the ϵ_{∞} is approximately 2.1; the total dielectric constant is 10% higher than experiment, though still of generally acceptable quality in comparison with several fixed-charge models.^{90–94} We note that the optical dielectric is slightly higher than the value for TIP4P-FQ reported by Rick et al.,¹ as well as experimental estimates. However, the value estimated for TIP4P-FQ using the present approach, $\epsilon_{\infty} = 1.775$, overestimates the previously reported result of $\epsilon_{\infty} = 1.592$. This suggests the tendency for the Kirkwood approach to overestimate the optical dielectric constant. The increased value of the optical dielectric constant for TIP4P-QDP over that of TIP4P-FQ is attributed to the higher molecular polarizability, which influences ϵ_{∞} as dictated by the Clausius–Mossotti relation.

On the basis of the results of QDP-P1 which yielded $\epsilon \approx 98$, it is suggested that the average condensed phase dipole moment plays an important role in obtaining the correct dielectric constant. In this regard, we find that $\langle \mu_{\text{liq}} \rangle \approx 2.6$ is sufficient for the QDP model to approach the experimental dielectric constant—an observation also made by Sprik.⁸⁵ Therefore, the higher dielectric constant of TIP4P-QDP can be attributed to the slightly larger average dipole moment.

7. Diffusion Constant. The self-diffusion constant was calculated using the Einstein relationship applied to constant volume and temperature simulations of pure liquid:

$$D_s = \lim_{t \rightarrow \infty} \frac{1}{6t} \langle (r(t) - r(0))^2 \rangle \quad (15)$$

The volume of the simulation cell was set to reproduce the average density of TIP4P-QDP from the constant *NPT* simulations. The diffusion constant for TIP4P-QDP was calculated to be $2.20 (\pm 0.04) \times 10^{-9}$ m²/s which is quite close to the experimental value of 2.30×10^{-9} m²/s. This

Table 5. Condensed Phase and Interfacial Properties

property	TIP4P-FQ ^a	TIP4P-QDP	QDP-P1	experiment
ρ_{liq} (g/cm ³)	1.0001 (0.0003)	0.9954 (0.0002)	0.9951 (0.0002)	0.997 ^b
$\langle\mu_{\text{liq}}\rangle$ (Debye)	2.623 (0.001)	2.641 (0.001)	2.752 (0.001)	2.96 (0.60) ^c
ΔH_{vap} (kcal/mol)	10.49 ^d	10.55 (0.12)	10.96 (0.12)	10.51 ^b
$\langle\alpha_{\text{iso,liq}}\rangle$ Å ³	1.12 ^d	1.309 (0.001)	1.323 (0.001)	1.34 ^e
D_s (10 ⁻⁹ m ² /s) ^j	1.93 (0.05), 2.15	2.20 (0.04), 2.46	1.83(0.05), 2.04	2.30 ^f
κ_T (10 ⁻¹⁰ Pa ⁻¹)	3.877 (0.098)	4.013 (0.062)	3.409 (0.051)	4.524 ^b
C_P (cal/mol K)	21.0 (5.5)	16.4 (3.5)	18.5 (2.2)	18.0 ^b
ϵ_∞	1.775, 1.592 ^d	2.128	2.057	1.79 ^g
ϵ	79. (8) ^d	85.8 (1.0)	97.6 (0.2)	78. ^h
$\Delta\Phi$ (kcal/mol)	-12.21 (0.05)	-11.98 (0.08)	-12.87 (0.05)	
γ (dyne/cm)	72.7 (1.5)	71.0 (2.7)	81.2 (3.1)	71.9 ⁱ

^a Values presented are based on calculations from this work, unless otherwise noted. ^b Reference 116. ^c Reference 78. ^d Reference 1.

^e Estimated condensed-phase isotropic polarizability based on the gas-phase value of 1.47 Å³ from ref 114 and assuming a 9% reduction in polarizability as deduced by Morita in ref 74. ^f Reference 117. ^g Reference 118. ^h Reference 119. ⁱ Reference 120. ^j Values as calculated for an $N = 216$ system (left) and corrected for extrapolation to infinite system size (right).

reflects an improvement over TIP4P-FQ calculated here to be $1.93 (\pm 0.05) \times 10^{-9}$ m²/s and elsewhere¹ to be $1.9 (\pm 0.1) \times 10^{-9}$ m²/s. As previously mentioned, the enhanced diffusion constant relative to TIP4P-FQ is likely to be the result of reduced structure in the condensed phase as suggested by decreased hydrogen bonding. We mention the diffusion constant calculated for QDP-P1 was lower than both TIP4P-QDP and TIP4P-FQ. It is reasoned that the enhanced dipole moment of QDP-P1 is influenced by higher cohesive intermolecular forces which limit the dynamics in the bulk. However, little change in the average hydrogen bonding relative to the TIP4P-QDP model suggests that the strong cohesive interactions did not result in enhanced organization of the fluid structure. From the QDP-P1 RDF, it is evident that QDP-P1 lacks key structural features that are common to both TIP4P-QDP and TIP4P-FQ, in particular the depletion of the first minimum in the O–O distribution.

Finally, it has been suggested that diffusion constants computed from molecular dynamics simulations have an inherent sensitivity to system size.⁹⁹ Hence, in order to make a valid comparison to experimental data, the diffusion constant should be extrapolated for an infinitely large system. Simulations of a larger system ($N = 988$) of TIP4P-QDP were performed to assess the extent to which system size influenced the calculation. For this larger system, a diffusion constant of $2.40 (\pm 0.02) \times 10^{-9}$ m²/s was calculated. Employing the linear extrapolation method used by Miller and Manolopoulos,⁹⁹ we estimate the diffusion constant for an infinitely large system to be approximately 2.46×10^{-9} m²/s, suggesting a 1.1 scaling factor from the $N = 216$ to the $N = \infty$ system. Applying this factor to the TIP4P-FQ and TIP4P-QDP values yields better agreement with the experimental value. Although the corrected diffusion constant of TIP4P-QDP now overestimates experiment, the deviation from experiment is relatively consistent with the uncorrected value. The diffusion constants as calculated for the $N = 216$ system and extrapolated for $N = \infty$ are included in Table 5.

8. Isobaric Heat Capacity. The isobaric heat capacity was calculated via numerical differentiation method utilized by Horn et al.⁹¹

$$C_P = \left(\frac{\partial H}{\partial T} \right)_P \approx \frac{\langle H_2 \rangle - \langle H_1 \rangle}{T_2 - T_1} \quad (16)$$

where $\langle H \rangle$ is the average enthalpy calculated from NPT

simulations. Additional simulations at $T = 297$ and 299 K were utilized to compute C_P at 298 K. TIP4P-QDP has a heat capacity of $16.4 (\pm 3.5)$ which underestimates experiment by about 9%. This agreement with experiment is slightly better than TIP4P-FQ, which overestimates experiment by about 17%. It is further noted that eq 16 provides only an approximate C_P value that is not corrected for quantum effects. Regardless, such effects are not expected to greatly influence the results reported here since they are anticipated to be less than the magnitude of uncertainty for each value.

9. Isothermal Compressibility. The isothermal compressibility was calculated using the following equation:

$$\kappa_T = \frac{\sigma_v^2}{\langle V \rangle k_B T} \quad (17)$$

where $\langle V \rangle$ and σ_v denote the average and the standard deviation of the total system volume over the course of the simulation, T is the temperature, and k_B represents Boltzmann's constant. For TIP4P-QDP, a value of $4.013 (\pm 0.062) \times 10^{-10}$ Pa⁻¹ was calculated. Although this is 0.5×10^{-10} Pa⁻¹ lower than the experimental value, it showed a 3% improvement over the value calculated for TIP4P-FQ. As is anticipated due to the dependence of this property on σ_v , QDP-P1 exhibited a value of $\kappa_T \approx 3.3$, which is notably less than both the TIP4P-QDP and TIP4P-FQ. The reduced value of κ_T results from reduced fluctuations in volume, a characteristic expected from increased cohesive forces resulting from the enhanced dipole moments as previously suggested.

C. Liquid–Vapor Interfacial Properties. 1. Density Profile. The water density profiles as a function of the z -position relative to the center of mass of the water slab are presented in Figure 4. From this data, the Gibbs dividing surface (GDS) is calculated to occur at 26.01 Å³ from the system's center of mass for both TIP4P-QDP and TIP4P-FQ. The GDS is calculated as the point in which the surface excess is zero. Using the “10–90” criteria for interfacial thickness,¹⁰⁰ the interfacial region is considered to be the region in which the density transitions from 10% to 90% of the bulk condensed-phase density. We estimate the interfacial thickness to be approximately 3.3 Å for TIP4P-QDP which is commensurate with that for TIP4P-FQ in this work. The TIP4P-FQ interfacial thickness has been previously reported

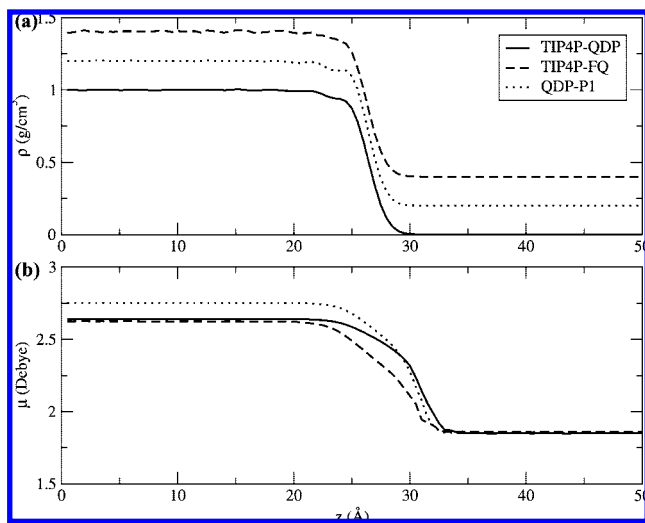


Figure 4. Interfacial profiles as a function of z -position relative to the center of mass for (a) the density and (b) the dipole moment of TIP4P-QDP, TIP4P-FQ, and QDP-P1. A 0.2 g/cm³ offset was applied to the density profiles to distinguish unique features.

as 3.5 Å,¹⁰¹ which agrees reasonably well with the value calculated here. One notable difference between the density profiles of the two models is a distinguishable “notch” present in the TIP4P-QDP profile at the onset of the interfacial region. This notch represents a region prior to the onset of the interface, but features a reduced density of approximately 0.93 g/cm³. This notch is a feature that was also observed for QDP-P1. While the TIP4P-FQ profile shows a region of reduced density between the pure bulk phase and interface, this region features a gradual slope, different than the sharp drop-off and leveling observed in the QDP models. This suggests that the introduction of dynamical polarizability allows for the formation a stable transitional region between the condensed phase and interface (as defined by the 10–90 criteria). The nature of hydrogen bonding (see also section III.C.3) between the two models at this depth is reasoned to cause this feature. While a general trend of decreasing hydrogen bonds beginning at the onset of this region is observed for both model types, the ratio of hydrogen bonds to the coordination number becomes notably higher for the QDP models than TIP4P-FQ at this depth. Additional spatial requirements for hydrogen bond networking, as well as the increased stability of such a network help explain this region of reduced density exhibited by the QDP models.

2. Dipole Moment Profile. The dipole moment profile is presented in Figure 4 for TIP4P-QDP and TIP4P-FQ. Consistent with the condensed-phase simulations, the average condensed-phase dipole moment is approximately 2.641(±0.001) D for TIP4P-QDP, which is slightly higher than the TIP4P-FQ value of 2.623 (±0.001) D. The enhanced TIP4P-QDP dipole moments in the region extending from the interface into the gas-phase are an anticipated result from the increasing molecular polarizability in this region relative to the bulk phase. It is noted, however, that the dipole moment of both models ultimately reduce to the appropriate value of 1.85 Debye within the gas-phase. Furthermore, this dipole moment enhancement suggests hydrogen bond net-

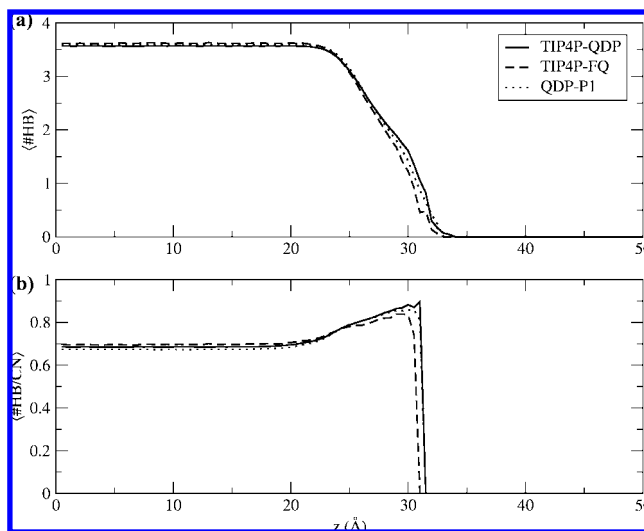


Figure 5. Hydrogen bond profile. (a) Average number of hydrogen bonds as a function of z -position for TIP4P-QDP, TIP4P-FQ, and QDP-P1. (b) Probability of hydrogen bond formation as a function of z -position as calculated from the ratio of hydrogen bonds to coordination number. Definitions of O–O distance less than 3.5 Å and H–O–O angle less than 30° were used as the hydrogen bond criteria.

works extending into the gas-phase as supported in the following section. Similar results were seen in QDP-P1, suggesting this is a common effect due to the modulation of polarizability in this region.

3. Hydrogen Bond Profile. For the hydrogen bond profile (Figure 5), the average number of hydrogen bonds formed by a water molecule as a function of its z -position relative to the center of mass was calculated. The definition for a hydrogen bond was based on the geometric criteria used by Liu et al.¹⁰¹ We select the geometric definition over an energetic one¹⁰² such that a comparison could be drawn to the results of Liu et al. and because this definition has shown more reliable simulation results.¹⁰³ Using an O–O distance of 3.5 Å as a distance criteria, prospective hydrogen bonding pairs were tagged. Among these tagged pairs, an angular requirement for the HO–O bond to be less than 30° was implemented to define a hydrogen bond pair. Within the bulk region, water molecules formed an average of 3.57 hydrogen bonds for TIP4P-QDP while the average for TIP4P-FQ was 3.62 hydrogen bonds. Also presented in Figure 5 is the probability of hydrogen bond formation as a function of z -position relative to the center of mass. This probability was calculated as the ratio of the number of hydrogen bonds formed by a molecule divided by its coordination number. The coordination number was defined as the number of water molecules having an O–O distance less than 3.5 from the water molecule of consideration. The probability of hydrogen bond formation increases significantly in the interfacial region compared to the bulk for both models. This is consistent with the observations of Liu et al. for TIP4P-FQ.¹⁰¹ It is noted, however, that the hydrogen bond probability for TIP4P-QDP is reduced in the condensed phase and enhanced in the interfacial region, relative to TIP4P-FQ. This reduced hydrogen bonding within the condensed region was anticipated based on the reduced structure indicated by the RDFs

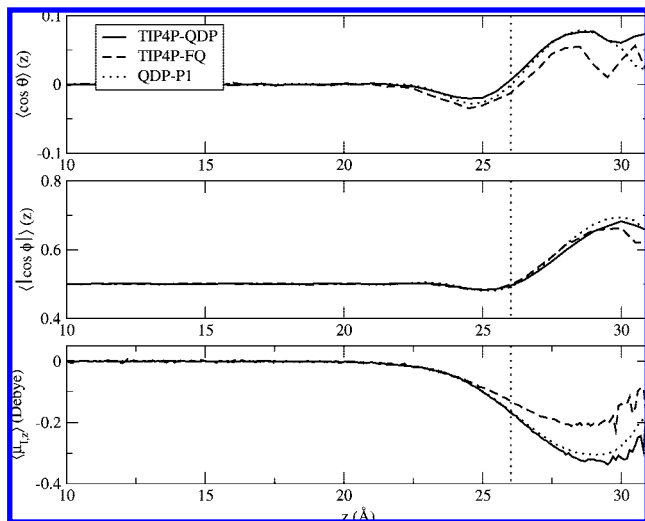


Figure 6. (a) Profile of $\langle \cos \theta \rangle$, where θ is angle formed between the permanent dipole vector of the water molecule and the fixed z -axis. (b) Profile of $\langle \cos \phi \rangle$, where ϕ is the angle formed between the molecular plane of water and the fixed z -axis. (c) Profile of the z -induced dipole moment. All z -values are relative to the center of mass of the system. The GDS is represented on each plot as a dashed vertical line.

of TIP4P-QDP. It is likely the combination of enhanced polarizability relative to the bulk and a more favorable dimer energy than TIP4P-FQ prolong a water molecule's ability to remain hydrogen bonded as it leaves the interface for the gas-phase.

4. Molecular Orientation. The orientational structure of TIP4P-QDP and TIP4P-FQ are analyzed via the distribution of two angular coordinates, θ and ϕ , as a function of z -position with respect to the GDS. For convenience, we present the orientational distributions as a function of the average value of the cosine of these angles. The angle θ is defined here as the angle between the permanent molecular dipole vector (as determined from the gas-phase dipole moment) and the fixed z -axis of the simulation cell (the vector perpendicular to the surface). For molecules below the GDS in which $\theta = 0^\circ$, both hydrogen sites are directly pointing toward the gas-phase. Molecules having $\theta = 90^\circ$ are those in which the molecular symmetry axis is parallel to the surface. The second angular component under consideration, ϕ is the angle made between the molecular plane and the z -axis of the simulation cell. A value $\cos \phi = 0$ represents a molecule lying parallel to the GDS, while $\cos \phi = \pm 1$ represents configurations perpendicular to the GDS. Due to the indistinguishability of the two perpendicular configurations, the absolute value of this quantity is considered.

The orientational profiles with respect to the depth relative to the GDS are presented in Figure 6. The $\langle \cos \theta \rangle$ profile suggests TIP4P-QDP has a stronger orientational preference than for the molecules' permanent dipole vector in the outermost portion of the interface than TIP4P-FQ. There is, however, a diminished orientational preference for TIP4P-QDP within the condensed phase. This profile suggests hydrogen atoms point into the gas-phase for values of z above the GDS, while there is a lesser preference for hydrogen atoms to point into solution below the GDS. Furthermore,

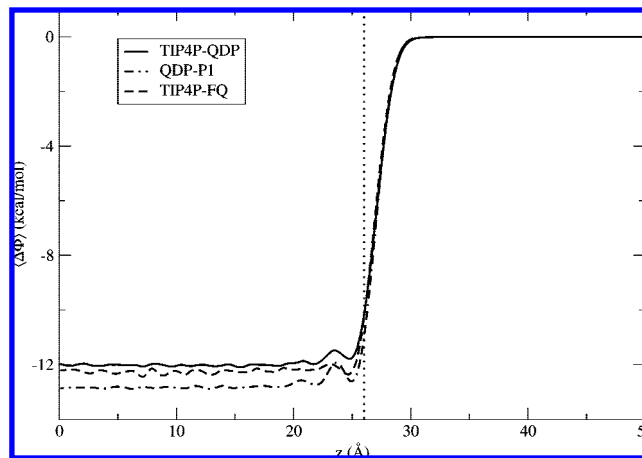


Figure 7. Total interfacial potential as a function of z relative to the center of mass of the water slab.

there is essentially no orientational preference in the condensed-phase region ($\langle \cos \theta \rangle$), which is expected from the bulk isotropic environment. The $\langle \cos \phi \rangle$ profile demonstrates similar features. Within the condensed-phase region, there is essentially no net structural effect (a value of 0.5 represents the average of the two extreme values for this property). Again, a notable well forms in the region several angstroms below the GDS in the $\langle \cos \phi \rangle$ profile, suggesting a strong preference for the water to lie parallel to the surface but slightly tipped such that the hydrogens point toward the bulk. A peak in this profile above the GDS indicates a preference for the water molecule to orient perpendicular to the surface; this preference is essentially the same for the different models.

Within the context of orientation profiles, the z -induced dipole moment can also be discussed. The z -induced dipole moment was calculated by subtracting the fixed z -component of the dipole moment for the z -projection of the total dipole moment for each molecule. The profile of this quantity as a function of z -position relative to the center of mass is also featured in Figure 6. There is significant (over 50%) increase in the maximum induced dipole moment for TIP4P-QDP over TIP4P-FQ. This increase is expected based on the increased θ preference of the TIP4P-QDP model since θ is connected to the permanent dipole moment vector.

5. Interfacial Potential. The interfacial potential is the potential drop associated with moving a volumeless positive test charge from the vapor phase into solution. This is a measure of the combined electrostatic effects of the water orientation and induced dipole moment distributions at the interface. The liquid–vapor interfacial potential is calculated by the integration of z -component of charge density^{11,33,66,69,104} $\rho(z)$, as

$$\Delta\Phi(z) = \Phi(z) - \Phi(z_0) = - \int_{z_0}^z dz' \int_{z_0}^{z'} dz'' \rho(z) \quad (18)$$

where z is the direction perpendicular to the interface and z_0 is center of mass position of the bulk phase. The integration is performed numerically by evaluation of the charge density for 1 Å-wide segments in the z -direction. The interfacial potential for TIP4P-QDP converges to $-11.98 (\pm 0.08)$ kcal/

mol, while a more favorable potential of $-12.21 (\pm 0.05)$ kcal/mol is calculated for TIP4P-FQ. Currently, there is no experimental consensus on the value, or even the sign of interfacial potential since values have been presented in the range ± 1500 mV (± 34.6 kcal/mol).^{105,106} Furthermore, we remark that studies of the aqueous liquid–vapor interface utilizing molecular dynamics have reported more consistent values in the range of -400 to -600 mV (approximately -9 to -14 kcal/mol).^{54,69,107–110} We note that the values calculated for all water models in this study fall in the typical range for MD simulations, with the TIP4P-FQ value demonstrating excellent agreement with the previously reported value of $12.20 (\pm 0.05)$ kcal/mol.¹¹⁰ Integration of charge density allows for the partitioning of the interfacial potential into dipole and quadrupole moment contributions.¹⁰ The similar dipole contributions for the two models, approximately 13.74 kcal/mol, indicate the quadrupole contributions offer the greatest differences between the models. The interfacial potential profile for TIP4P-QDP and TIP4P-FQ is featured in Figure 7. A distinguishing feature of the TIP4P-QDP profile is the exaggerated peak in the region just below the interface, which based on the aforementioned comments is likely a consequence of a locally enhanced quadrupole moment contribution.

6. *Surface Tension.* As a final comparison between the TIP4P-QDP and TIP4P-FQ models in the liquid–vapor interface, the surface tension was calculated from the difference of the normal and tangential elements of the internal pressure tensor¹¹¹

$$\gamma(z) = \frac{L_z}{2} \left(P_{zz} - \frac{P_{xx} + P_{yy}}{2} \right) \quad (19)$$

where P_{xx} , P_{yy} , and P_{zz} are the diagonal elements of the internal pressure tensor and L_z is the length of the simulation cell in the z -direction (normal to the surface). Surface tension computed for TIP4P-QDP model is $71.0 (\pm 2.7)$ dyne/cm, 2.3% less than the TIP4P-FQ estimate of 72.7 dyne/cm and 1.3% less than the experimental value of 71.9 dyne/cm. This slight reduction is consistent with the more favorable dimer energy than TIP4P-FQ which allows a reduced energetic penalty for water molecules leaving the condensed phase for the vapor phase.

IV. Conclusions

In this work, we have presented a new water model, TIP4P-QDP, which explicitly accounts for the polarizability gradient between thermodynamic phases. The model is built upon the charge equilibration formalism and the TIP4P-FQ model of Rick et al.¹ Although there are numerous possible paths to introduce phase-dependence in the context of molecular dynamics simulations, we chose the development of a multiplicative scaling function that is based on the M -site partial charge. This notion is based on the considerable gradient in dipole moment from gas to liquid phases, which could be coupled to a change in molecular polarizability between these two phases. An error function was chosen as the functional form due to its ability to apply constant scaling in regions considered purely gaseous or condensed, while providing

nearly linear modulation between these two phases. Moreover, atomic electronegativities were also scaled in order to maintain self-consistency with the hardness scaling. Here additional scaling parameter, p , was used to control the amount by which χ was scaled. Although a value of $p = 1$ is expected to reduce the charge-dependent expressions to their charge-independent analogs for an isolated molecule, condensed phase effects result in undesirable increases in cohesive forces. Hence, a reduced p -value allowed for an appropriate average condensed-phase dipole moment and an accurate depiction of intermolecular forces in the condensed phase as suggested by the agreement of these properties with experiment.

A reparameterization of the hardness, electronegativity, and Lennard-Jones parameters was necessary to correct the gas phase polarizability, dipole moment, and dimer energies. Selection of the specific parameter set was based on the ability to simultaneously match the density and enthalpy of vaporization to experiment. Ultimately, the density at ambient conditions, $0.9954 (\pm 0.0002)$ g/cm³, and enthalpy of vaporization, $10.55 (\pm 0.12)$ kcal/mol, demonstrate excellent agreement with experiment. Isothermal compressibility, diffusion constants, and isobaric heat capacity are also commensurate with the experimental and TIP4P-FQ results. The dielectric constant of $\epsilon = 85.8$ overestimates experiment by 10%. However, the comparison of TIP4P-QDP as presented in this work to its analog with full scaling on χ ($p = 1$) suggests that the average dipole moment in the condensed phase is an important consideration for replicating the appropriate dielectric constant. Interfacial properties are qualitatively similar to the TIP4P-FQ results. Consistent observations made among *charge*-dependent models with different p -values suggest features that are a direct consequence of accounting for the polarizability gradient between phases. A hydrogen bond network that extends further into the gaseous region than TIP4P-FQ, as well as a corresponding extension of enhanced dipole moments, suggest enhanced cohesion within the interfacial region. This is anticipated on the basis of increased polarizability and more favorable dimer energy of the TIP4P-QDP model. A stronger orientational preference of the TIP4P-QDP model's permanent dipole vector is also a common feature of the QDP-scheme that results in an enhanced z -induced dipole moment.

Acknowledging that the scaling function used for TIP4P-QDP is not rigorously bound to experimental or quantum mechanical results, we stress that the primary focus of this work is a preliminary analysis of how accounting for the difference in polarizability between phases affects the physics of the liquid–vapor interface. Furthermore, relationships dictating the nature of change of polarizability via a convenient simulation parameter such as Q_M are not definite, limiting the level to which this model can replicate such phenomena. The coupling of the scaling function to the M -site charge is a computationally efficient and convenient method of incorporating a phase-dependent molecular polarizability in molecular dynamics simulations. Future generations of phase-dependent models may rely on hydrogen

bond coordination, which has been shown to correspond strongly to both the molecular dipole moment^{95,96} and molecular polarizability.⁷⁵

The first step toward exploring the implications of such physics within the context of classical molecular dynamics simulations, we have demonstrated an approach to incorporate phase dependence of molecular polarizability. The resulting TIP4P-QDP model also demonstrates intriguing physical properties, most notably, the enhanced structure of the liquid–vapor interface. One promising approach toward improving this model will be to introduce an additional scaling of the Lennard-Jones parameters.¹¹² Such modifications may capture more precise structural features that were ignored in the current treatment. This may in turn further improve upon the condensed-phase properties calculated here. Future incorporation of additional atomic sites will allow for treatment of out of plane polarizability, a feature neglected in the original TIP4P-FQ model and the TIP4P-QDP model proposed in this work. Future studies involving TIP4P-QDP (or further refined versions of this model) will focus on how phase-dependent polarizability affects interfacial simulations involving nonpolarizable and polarizable ions. Furthermore, the extent to which this model can replicate the liquid–vapor coexistence curve will also be studied. The dynamical nature of polarizability as exhibited in TIP4P-QDP is a crucial element that has been lacking in studies involving the latter, and it is therefore suggested that the TIP4P-QDP model (and future versions) may have success in such applications.

Acknowledgment. The authors gratefully acknowledge support from the National Institute of Health sponsored COBRE (Center of Biomedical Research) Grant P20-RR015588 (Department of Chemical Engineering) at the University of Delaware. One of the authors, S.P., also acknowledges the University of Delaware for startup funds.

Appendix: Derivation of QDP Expressions

The charge-dependent polarizable water model introduces a multiplicative scaling factor to each term in the Hamiltonian. In addition to the Q -dependent scaling it is desired to control the magnitude of scaling on the χ parameter, which is done by the introduction of an empirical p -parameter. The generalized energy expression with Q -dependent hardness and Q, p -dependent electronegativities is given by

$$E(\mathbf{Q}) = \langle \chi(\mathbf{Q}, p) | \mathbf{Q} \rangle + \frac{1}{2} \langle \mathbf{Q} | \mathbf{J}(\mathbf{Q}, \mathbf{r}) | \mathbf{Q} \rangle \quad (\text{A1})$$

By taking a derivative with respect to the k th charge and setting the resulting expression

$$\nabla_k E(\mathbf{Q}) = \chi_k(\mathbf{Q}, p) + \langle \mathbf{J}_k(\mathbf{Q}, \mathbf{r}) | \mathbf{Q} \rangle + \left\langle \nabla_k \chi(\mathbf{Q}, p) + \frac{1}{2} \mathbf{Q} [\nabla_k \mathbf{J}(\mathbf{Q}, \mathbf{r})] | \mathbf{Q} \right\rangle \quad (\text{A2})$$

equal to zero, we may obtain a set of simultaneous equations, one for each charge. In the above equation, χ_k is the k th site electronegativity and \mathbf{J}_k is the k th row of the hardness matrix.

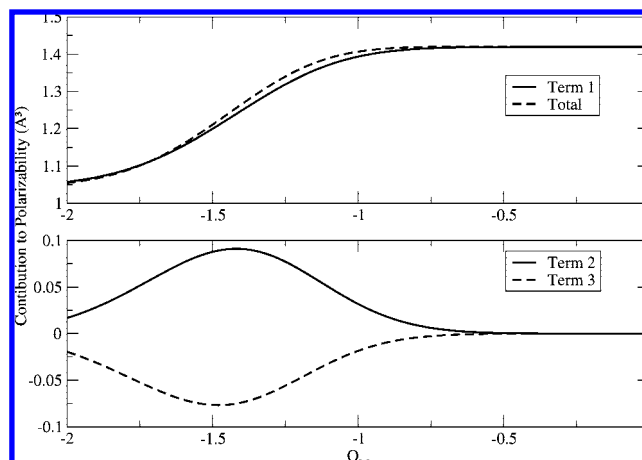


Figure 8. Contribution of each term in eq A18 to the total scaling function, $g(Q_M)$. The top panel features the first term of eq A18 (solid line) as it compares to the total scaling function (dashed line) as a function of Q_M . The lower panel features the second (solid line) and third (dashed line) terms of eq A18. Terms 2 and 3 are approximately equal in magnitude while opposite in sign, which results in the first term's dominance in $g(Q_M)$.

The first two terms in the above expression are the usual terms one obtains when χ and \mathbf{J} are independent of \mathbf{Q} . The last term accounts for the charge dependence of χ and \mathbf{J} . We may now make the specific assumptions

$$\chi(\mathbf{Q}, p) = \chi[(1 - p) + pg(Q_M)] \quad (\text{A3})$$

and

$$\mathbf{J}(\mathbf{Q}, \mathbf{r}) = \mathbf{J}(\mathbf{r})g(Q_M) \quad (\text{A4})$$

which tie the scaling of the hardnesses and electronegativities to a factor $g(Q_M)$ based on the M -site partial charge. Introduction of the p dependence in eq A3 acts to control the extent of scaling due to the $g(Q_M)$ term; a value of $p = 0$ introduces no Q_M -scaling, while a value of $p = 1$ introduces full scaling equivalent to that applied to the hardness matrix.

If we now consider a single water molecule and the cases in which k corresponds to a hydrogen site, only the first two terms of eq A2 survive (since χ and \mathbf{J} only depend on Q_M) and we may write

$$-\chi_H[(1 - p) + pg(Q_M)] = g(Q_M) \langle \mathbf{J}_H(\mathbf{r}) | \mathbf{Q} \rangle \quad (\text{A5})$$

Letting $h(Q_M) = g(Q_M)/[(1 - p) + pg(Q_M)]$ and rearranging, we obtain the simplified expression

$$-\chi_H = h(Q_M) \langle \mathbf{J}_H(\mathbf{r}) | \mathbf{Q} \rangle \quad (\text{A6})$$

which, in the limit $p = 1$, reduces to the usual expression

$$-\chi_H = \langle \mathbf{J}_H(\mathbf{r}) | \mathbf{Q} \rangle \quad (\text{A7})$$

For the M -site ($k = M$) and using the fact that $\nabla_M[(1 - p) + pg(Q_M)] = p \nabla_M g(Q_M)$, we obtain

$$-\chi_M = h(Q_M) \langle \mathbf{J}_M(\mathbf{r}) | \mathbf{Q} \rangle + \left[h(Q_M) \left(\frac{\nabla_M g(Q_M)}{g(Q_M)} \right) \times \left(p \chi_M \langle \hat{\mathbf{M}} | + \frac{1}{2} \langle \mathbf{Q} | \mathbf{J}(\mathbf{r}) | \right) | \mathbf{Q} \right] \quad (\text{A8})$$

where $\langle \hat{\mathbf{M}} |$ is a unit vector that picks out the M -site charge. The full system of equations is constructed from the equations for both hydrogen sites and the M -site as

$$-|\chi\rangle = h(Q_M) \left[\mathbf{J}(\mathbf{r}) + \left(\frac{\nabla_M g(Q_M)}{g(Q_M)} \right) \times \left(p\chi_M \mathbf{M} + \frac{1}{2} |\hat{\mathbf{M}}\rangle \langle \mathbf{Q} | \mathbf{J}(\mathbf{r}) | \right) \right] |\mathbf{Q}\rangle = h(Q_M) \mathbf{H}(\mathbf{Q}, \mathbf{r}) |\mathbf{Q}\rangle \quad (\text{A9})$$

where the matrix \mathbf{M} denotes the outer product $|\hat{\mathbf{M}}\rangle \langle \hat{\mathbf{M}}|$. This form allows us to recover eqs A6 and A8 upon dotting a particular unit vector such as $\langle \hat{\mathbf{M}} |$, $\langle \hat{\mathbf{H}}_1 |$, or $\langle \hat{\mathbf{H}}_2 |$ into this expression from the left. To compute the polarizability, we make the assumption

$$\mathbf{H}(\mathbf{Q}, \mathbf{r}) \approx \mathbf{H}(\langle \mathbf{Q} \rangle, \mathbf{r}) \quad (\text{A10})$$

which constructs a static (charge-independent) version of the hardness matrix from the true equilibrium charges. In the limit of no external field and $p = 1$ ($h(Q_M) = 1$), this assumption is exact since the same equilibrium charges are recovered and self-consistent:

$$\begin{aligned} h(Q_M) \mathbf{H}(\langle \mathbf{Q} \rangle, \mathbf{r}) |\mathbf{Q}\rangle &= -|\chi\rangle \\ \langle \mathbf{Q} \rangle &= -[\mathbf{H}(\langle \mathbf{Q} \rangle, \mathbf{r})]^{-1} |\chi\rangle \end{aligned} \quad (\text{A11})$$

In the presence of an external field, this assumption essentially requires that the charge-induced changes to the hardness matrix be small which should be a valid approximation in the weak field limit. This makes it unnecessary to iteratively solve the nonlinear system of equations. Therefore, the equilibrium charges in the presence of some external field ϵ_γ are given by

$$\begin{aligned} h(Q_M) \mathbf{H}(\langle \mathbf{Q} \rangle, \mathbf{r}) |\mathbf{Q}\rangle_\epsilon &\approx -|\chi\rangle + \frac{1}{g(Q_M)} \epsilon_\gamma |\mathbf{R}_\gamma\rangle \\ \langle \mathbf{Q} \rangle_\epsilon &\approx -[h(Q_M) \mathbf{H}(\langle \mathbf{Q} \rangle, \mathbf{r})]^{-1} |\chi\rangle + \left(\frac{[\mathbf{H}(\langle \mathbf{Q} \rangle, \mathbf{r})]^{-1}}{g(Q_M) h(Q_M)} \right) |\epsilon_\gamma \mathbf{R}_\gamma\rangle \end{aligned} \quad (\text{A12})$$

The induced dipole in the β direction is given by the difference in charges due to the presence of the field

$$\begin{aligned} \mu_\beta^{\text{ind}} &= \langle \mathbf{R}_\beta | \mathbf{Q} \rangle_\epsilon - \langle \mathbf{R}_\beta | \mathbf{Q} \rangle \approx \\ &\langle \mathbf{R}_\beta | \frac{[\mathbf{H}(\langle \mathbf{Q} \rangle, \mathbf{r})]^{-1}}{g(Q_M) h(Q_M)} |\epsilon_\gamma \mathbf{R}_\gamma\rangle \end{aligned} \quad (\text{A13})$$

and the derivative of the induced dipole moment with respect to the field then yields the $\beta\gamma$ component of the polarizability:

$$\alpha_{\beta\gamma}(Q_M) = \frac{\partial \mu_\beta^{\text{ind}}}{\partial \epsilon_\gamma} \approx \frac{1}{g(Q_M) h(Q_M)} \langle \mathbf{R}_\beta | [\mathbf{H}(\langle \mathbf{Q} \rangle, \mathbf{r})]^{-1} | \mathbf{R}_\gamma \rangle \quad (\text{A14})$$

By manipulating the definition of $\mathbf{H}(\mathbf{Q}, \mathbf{r})$ in eq A9, we may obtain an expression for the inverse as

$$[\mathbf{H}(\mathbf{Q}, \mathbf{r})]^{-1} = \mathbf{J}^{-1}(\mathbf{r}) \left[1 + \left(\frac{\nabla_M g(Q_M)}{g(Q_M)} \right) \times \left(p\chi_M \mathbf{M} \mathbf{J}^{-1}(\mathbf{r}) + \frac{1}{2} |\hat{\mathbf{M}}\rangle \langle \mathbf{Q} | \right) \right]^{-1} \quad (\text{A15})$$

which relates the charge-dependent hardness matrix to the charge-independent hardness matrix at leading order. Assuming the correction is small, we can perform a series expansion of the bracketed term to yield

$$[\mathbf{H}(\mathbf{Q}, \mathbf{r})]^{-1} = \mathbf{J}^{-1}(\mathbf{r}) \left[1 - \left(\frac{\nabla_M g(Q_M)}{g(Q_M)} \right) \times \left(p\chi_M \mathbf{M} \mathbf{J}^{-1}(\mathbf{r}) + \frac{1}{2} |\hat{\mathbf{M}}\rangle \langle \mathbf{Q} | \right) \right] \quad (\text{A16})$$

Insertion of this definition into the polarizability expression yields

$$\alpha_{\beta\gamma}(Q_M) \approx \frac{1}{g(Q_M) h(Q_M)} \left\langle \mathbf{R}_\beta | \mathbf{J}^{-1}(\mathbf{r}) \left[1 - \left(\frac{\nabla_M g(Q_M)}{g(Q_M)} \right) \times \left(p\chi_M \mathbf{M} \mathbf{J}^{-1}(\mathbf{r}) + \frac{1}{2} |\hat{\mathbf{M}}\rangle \langle \mathbf{Q} | \right) \right] | \mathbf{R}_\gamma \right\rangle \quad (\text{A17})$$

which expresses the polarizability in terms of the original, unscaled matrix $\mathbf{J}(\mathbf{r})$. Thus, when the gradient of $g(Q_M)$ is zero (constant $g(Q_M)$) for $p = 1$ ($h(Q_M) = 1$), the new contribution disappears so that the usual expression is recovered to within a multiplicative constant depending on the constant scaling factor applied to the hardnesses. Since $\mathbf{J}(\mathbf{r})$ is symmetric, this expression may be further simplified into

$$\alpha_{\beta\gamma}(Q_M) \approx \frac{\langle \mathbf{R}_\beta | \mathbf{J}^{-1}(\mathbf{r}) | \mathbf{R}_\gamma \rangle}{g(Q_M) h(Q_M)} - \left(\frac{\nabla_M g(Q_M)}{[g(Q_M)]^2 h(Q_M)} \right) \times \left[p\chi_M \langle \mathbf{R}_\beta | \mathbf{J}^{-1}(\mathbf{r}) | \hat{\mathbf{M}} \rangle^2 + \frac{1}{2} \langle \mathbf{R}_\beta | \mathbf{J}^{-1}(\mathbf{r}) | \hat{\mathbf{M}} \rangle \langle \mathbf{Q} | \mathbf{R}_\gamma \rangle \right] \quad (\text{A18})$$

The first term is the usual polarizability expression, but scaled by a factor which becomes $1/g(Q_M)$ in the limit $p = 1$. The second term always *increases* the polarizability if χ_M is positive and the gradient is negative since the functions $g(Q_M)$ and $h(Q_M)$ are always positive. The last term works to decrease the polarizability with increasing magnitude of the dipole moment. While all terms should be included in order to accurately estimate the Q -dependent polarizability, the last two terms are typically an order of magnitude smaller than the first term and opposite in sign. The magnitude of each term as a function of Q_M is featured in Figure 8. Finally, we remark that eq 7 is a slightly modified form of eq A18, utilizing the substitutions $\alpha_{\beta\gamma} = \langle \mathbf{R}_\beta | \mathbf{J}^{-1}(\mathbf{r}) | \mathbf{R}_\gamma \rangle$ and $\mu_\gamma = \langle \mathbf{Q} | \mathbf{R}_\gamma \rangle$.

References

- (1) Rick, S. W.; Stuart, S. J.; Berne, B. J. *J. Chem. Phys.* **1994**, *101*, 6141.
- (2) Matsumoto, M.; Kataoka, Y. *J. Chem. Phys.* **1989**, *90*, 2390.
- (3) Matsumoto, M.; Kataoka, Y. *J. Chem. Phys.* **1988**, *88*, 3233.
- (4) Petersen, P. B.; Saykally, R. J. *J. Chem. Phys. Lett.* **2004**, *397*, 51.
- (5) Petersen, P. B.; Saykally, R. J. *Annu. Rev. Phys. Chem.* **2006**, *57*, 333.
- (6) Petersen, P. B.; Saykally, R. J.; Mucha, M.; Jungwirth, P. J. *Phys. Chem. B* **2005**, *109*, 10915.

- (7) Walker, D. S.; Richmond, G. L. *J. Am. Chem. Soc.* **2007**, *129*, 9446–9451.
- (8) Walker, D. S.; Richmond, G. L. *J. Phys. Chem. C* **2007**, *111*, 8321–8330.
- (9) Foster, K. L.; Plastring, R. A.; Bottenheim, J. W.; Shepson, P. B.; Finlayson-Pitts, B. J.; Spicer, C. W. *Science* **2001**, *291*, 471.
- (10) Wilson, M. A.; Pohorille, A.; Pratt, L. R. *J. Chem. Phys.* **1989**, *90*, 5211.
- (11) Wilson, M. A.; Pohorille, A.; Pratt, L. R. *J. Chem. Phys.* **1988**, *88*, 3281.
- (12) Shen, Y. R. *Nature* **1989**, *337*, 519.
- (13) Salafsky, J. S.; Eiseenthal, K. B. *Chem. Phys. Lett.* **2000**, *319*, 435.
- (14) Salafsky, J. S.; Eiseenthal, K. B. *J. Phys. Chem. B* **2000**, *104*, 7752.
- (15) Vrbka, L.; Mucha, M.; Minofar, B.; Jungwirth, P.; Brown, E. C.; Tobias, D. J. *Curr. Opin. Colloid Interface Sci.* **2004**, *9*, 67.
- (16) Kuo, I. W.; Mundy, C. J.; Eggiman, B. L.; McGrath, M. J.; Siepmann, J. I.; Chen, B.; Vieceli, J.; Tobias, D. J. *J. Phys. Chem. B* **2006**, *110*, 3738.
- (17) Kuo, I. W.; Mundy, C. J. *Science* **2004**, *303*, 658.
- (18) MacKerell, A. D., Jr. *J. Comput. Chem.* **2004**, *25*, 1584.
- (19) Breneman, C. M.; Wiberg, K. B. *J. Comput. Chem.* **1990**, *11*, 361.
- (20) Chirlian, L. E.; Fancl, M. M. *J. Comput. Chem.* **1987**, *8*, 894.
- (21) Wang, J.; Cieplak, P.; Kollman, P. A. *J. Comput. Chem.* **2000**, *21*, 1049.
- (22) Bucher, D.; Raugei, S.; Guidoni, L.; DalPeraro, M.; Rothlisberger, U.; Carloni, P.; Klein, M. L. *Biophys. Chem.* **2006**, *124*, 292.
- (23) Halgren, T. A.; Damm, W. *Curr. Opin. Struct. Bio.* **2001**, *11*, 236.
- (24) Patel, S.; Brooks, C. L., III. *Mol. Sim.* **2006**, *32*, 231.
- (25) Koch, D. M.; Peslherbe, G. H. *J. Phys. Chem. B* **2008**, *112*, 636.
- (26) Smith, D. E.; Dang, L. X. *J. Chem. Phys.* **1994**, *100*, 3757.
- (27) Dang, L. X.; Rice, J. E.; Caldwell, J.; Kollman, P. A. *J. Am. Chem. Soc.* **1991**, *113*, 2481–2486.
- (28) Perera, L.; Berkowitz, M. L. *Z. Phys. D* **1993**, *26*, 166–168.
- (29) Perera, L.; Berkowitz, M. L. *J. Chem. Phys.* **1992**, *96*, 8288.
- (30) Lamoureux, G.; Roux, B. *J. Phys. Chem. B* **2005**, *110*, 3308.
- (31) Grossfield, A.; Ren, P.; Ponder, J. W. *J. Am. Chem. Soc.* **2003**, *125*, 15671.
- (32) Dang, L. X. *J. Chem. Phys.* **1992**, *97*, 2659.
- (33) Dang, L. X.; Chang, T. M. *J. Chem. Phys.* **1997**, *106*, 8149.
- (34) Dang, L. X.; Chang, T. M. *J. Chem. Phys.* **2003**, *119*, 9851.
- (35) Ren, P.; Ponder, J. W. *J. Comput. Chem.* **2002**, *23*, 1497.
- (36) Anisimov, V. M.; Lamoureux, G.; Vorobyov, I. V.; Huang, N.; Roux, B.; Alexander, D.; MacKerell, J. J. *Chem. Theory Comput.* **2005**, *1*, 153.
- (37) Vorobyov, I. V.; Anisimov, V. M.; Alexander, D.; MacKerell, J. J. *J. Phys. Chem. B* **2005**, *109*, 18988.
- (38) Patel, S.; Brooks, C. L., III. *J. Comp. Chem.* **2004**, *25*, 1.
- (39) Rick, S. W.; Berne, B. J. *J. Am. Chem. Soc.* **1996**, *118*, 672.
- (40) Banks, J. L.; Kaminski, G. A.; Zhou, R.; Mainz, D. T.; Berne, B. J.; Friesner, R. A. *J. Phys. Chem. B* **1999**, *110*, 741.
- (41) Stern, H.; Kaminski, G. A.; Banks, J. L.; Zhou, R.; Berne, B. J.; Friesner, R. A. *J. Phys. Chem. B* **1999**, *103*, 4730.
- (42) Stern, H.; Rittner, F.; Berne, B. J.; Friesner, R. *J. Chem. Phys.* **2001**, *115*, 2237.
- (43) Kaminski, G. A.; Stern, H. A.; Berne, B. J.; Friesner, R. A. *J. Phys. Chem. A* **2004**, *108*, 621.
- (44) Kaminski, G. A.; Stern, H. A.; Berne, B. J.; Friesner, R. A.; Cao, Y. X.; Murphy, R. B.; Zhou, R.; Halgren, T. A. *J. Comput. Chem.* **2002**, *23*, 1515.
- (45) Ledecq, M.; Lebon, F.; Durant, F.; Giessner-Prettre, C.; Marquez, A.; Gresh, N. *J. Phys. Chem. B* **2003**, *107*, 10640.
- (46) Gresh, N. *J. Comput. Chem.* **1995**, *16*, 856.
- (47) Gresh, N.; Garmer, D. R. *J. Comput. Chem.* **1996**, *17*, 1481.
- (48) Patel, S.; MacKerell, A. D.; Brooks, C. L., III. *J. Comp. Chem.* **2004**, *25*, 1504.
- (49) Piquemal, J.-P.; Chevreau, H.; Gresh, N. *J. Chem. Theory Comput.* **2007**, *3*, 824.
- (50) Gresh, N.; Cisneros, G. A.; Darden, T. A.; Piquemal, J.-P. *J. Chem. Theory Comput.* **2007**, *3*, 1960.
- (51) Ren, P.; Ponder, J. W. *J. Phys. Chem. B* **2003**, *107*, 5933.
- (52) Caldwell, J. W.; Kollman, P. A. *J. Phys. Chem.* **1995**, *99*, 6208.
- (53) Vorobyov, I. V.; Anisimov, V. M.; Greene, S.; Moser, R. M. V. A.; Pastor, R. W.; Alexander, D.; MacKerell, J. J. *Chem. Theory Comput.* **2007**, *3*, 1120.
- (54) Lamoureux, G., Jr.; Roux, B. *J. Chem. Phys.* **2003**, *119*, 5185.
- (55) Lamoureux, G.; Roux, B. *J. Chem. Phys.* **2003**, *119*, 3025.
- (56) Mortier, W. J.; Ghosh, S. K.; Shankar, S. *J. Am. Chem. Soc.* **1986**, *108*, 4315.
- (57) Mortier, W. J.; Genechten, K. V.; Gasteiger, J. *J. Am. Chem. Soc.* **1985**, *107*, 829.
- (58) Rappé, A. K.; Goddard, W. A., III. *J. Phys. Chem.* **1991**, *95*, 3358.
- (59) Rick, S. W. *J. Chem. Phys.* **2001**, *114*, 2276.
- (60) Rick, S. W.; Stuart, S. J.; Bader, J. S.; Berne, B. J. *J. Mol. Liq.* **1995**, *65/66*, 31.
- (61) Olano, L. R.; Rick, S. W. *J. Comput. Chem.* **2005**, *26*, 699.
- (62) Patel, S.; Brooks, C. L., III. *J. Chem. Phys.* **2006**, *124*, 204706.
- (63) Nalewajski, R. F.; Korchowiec, J.; Zhou, Z. *Int. J. Quantum Chem.* **1988**, *22*, 349.
- (64) Patel, S.; Brooks, C. L., III. *J. Chem. Phys.* **2005**, *122*, 24508.
- (65) Ribeiro, M. C. C.; Almeida, L. C. J. *J. Chem. Phys.* **1999**, *110*, 11445.
- (66) Patel, S.; Brooks, C. L., III. *J. Chem. Phys.* **2005**, *123*, 164502.
- (67) Zhong, Y.; Warren, G. L.; Patel, S. *J. Comput. Chem.* **2008**, *29*, 1142.

- (68) Rick, S. W.; Stewart, S. J. Potentials and Algorithms for Incorporating Polarizability in Computer Simulations. In *Reviews of Computational Chemistry*; Lipkowitz, K. B. Boyd, D. B. Eds.; John Wiley & Sons: New York, 2002; p 89.
- (69) Dang, L. X.; Chang, T.-M. *J. Phys. Chem. B* **2002**, *106*, 235.
- (70) Yu, H.; Geerke, D. P.; Liu, H.; v. Gunsteren, W. F. *J. Comput. Chem.* **2006**, *27*, 1494.
- (71) Dang, L. X. *J. Phys. Chem. B* **2001**, *105*, 804.
- (72) Dang, L. X.; Chang, T. M.; Panagiotopoulos, A. Z. *J. Chem. Phys.* **2002**, *117*, 3522.
- (73) Piquemal, J.-P.; Perera, L.; Cisneros, G. A.; Ren, P.; Pedersen, L. G.; Darden, T. A. *J. Chem. Phys.* **2006**, *125*, 054511.
- (74) Morita, A. *J. Comput. Chem.* **2002**, *23*, 1466.
- (75) Krishtal, A.; Senet, P.; Yang, M.; van Alsenoy, C. *J. Chem. Phys.* **2006**, *125*, 034312.
- (76) Schropp, B.; Tavan, P. *J. Phys. Chem. B* **2008**, *112*, 6233.
- (77) Silvestrelli, P. L.; Parrinello, M. *Phys. Rev. Lett.* **1999**, *82*, 3308.
- (78) Badyal, Y. S.; Sabounji, M. L.; Price, D. L.; Shastri, S. D.; Haefner, D. R.; Soper, A. K. *J. Chem. Phys.* **2000**, *112*, 9206.
- (79) Sanderson, R. T. *Chemical Bonds and Bond Energy*; Academic Press: New York, 1976.
- (80) Sanderson, R. T. *Science* **1951**, *114*, 670.
- (81) Chelli, R.; Procacci, P. *J. Chem. Phys.* **2002**, *117*, 9175.
- (82) Itskowitz, P.; L. Berkowitz, M. *J. Chem. Phys.* **1997**, *101*, 5687.
- (83) Warren, G. L.; Davis, J. E.; Patel, S. *J. Chem. Phys.* **2008**, *128*, 144110.
- (84) Bauer, B. A.; Patel, S. *J. Mol. Liq.* **2008**, *142*, 32.
- (85) Sprik, M. *J. Chem. Phys.* **1991**, *95*, 6762.
- (86) Brooks, B. R.; Brucoleri, R. E.; Olafson, B. D.; Stages, D. J.; Swaminathan, S.; Karplus, M. *J. Comput. Chem.* **1983**, *4*, 187.
- (87) Brooks, C. L., III.; Karplus, M.; Pettitt, B. M. *A Theoretical Perspective of Dynamics, Structure, and Thermodynamics*; John Wiley & Sons: New York, 1988; Vol. LXXI.
- (88) Darden, T.; York, D.; Pedersen, L. *J. Chem. Phys.* **1993**, *98*, 10089.
- (89) Nose, S. *Mol. Phys.* **1984**, *52*, 255.
- (90) Jorgensen, W. L.; Chandrasekhar, J.; Madura, J. D.; Impey, R. W.; Klein, M. L. *J. Chem. Phys.* **1983**, *79*, 926.
- (91) Horn, H. W.; Swope, W. C.; Pitera, J. W.; Madura, J. D.; Dick, T. J.; Hura, G. L.; Head-Gordon, T. *J. Chem. Phys.* **2004**, *120*, 9665.
- (92) Price, D. J.; Brooks, C. L., III. *J. Chem. Phys.* **2004**, *121*, 10096.
- (93) Mahoney, M. W.; Jorgensen, W. L. *J. Chem. Phys.* **2000**, *112*, 8910.
- (94) Alper, H. E.; Levy, R. M. *J. Chem. Phys.* **1989**, *91*, 1242.
- (95) McGrath, M. J.; Siepmann, J. I.; Kuo, I. F. W.; Mundy, C. J. *Mol. Phys.* **2007**, *105*, 1411.
- (96) Kemp, D. D.; Gordon, M. S. *J. Phys. Chem. A* **2008**, *112*, 4885.
- (97) Soper, A. K.; Phillips, M. G. *Chem. Phys.* **1986**, *107*, 47.
- (98) Soper, A. K. *J. Phys.: Condens. Matter* **2007**, *19*, 335206.
- (99) Miller, T. F., III.; Manolopoulos, D. E. *J. Chem. Phys.* **2005**, *123*, 154504.
- (100) Beaglehole, D. *Fluid Interfacial Phenomena*; Wiley: New York, 1986.
- (101) Liu, P.; Harder, E.; Berne, B. J. *J. Phys. Chem. B* **2005**, *109*, 2949.
- (102) Benjamin, I. *Chem. Rev.* **1996**, *96*, 1449.
- (103) Starr, F.; Nielsen, J.; Stanley, H. *Phys. Rev.* **2000**, *62*, 579.
- (104) Pandit, S. A.; Bostick, D.; Berkowitz, M. L. *Biophys. J.* **2003**, *85*, 3120.
- (105) Parfenyuk, V. I. *Colloid J.* **2002**, *64*, 588.
- (106) Paluch, M. *Adv. Colloid Interface Sci.* **2000**, *84*, 27.
- (107) Warren, G. L.; Patel, S. *J. Chem. Phys.* **2007**, *064509*, 127.
- (108) Ishiyama, T.; Morita, A. *J. Phys. Chem. C* **2007**, *111*, 721.
- (109) Sokhan, V. P.; Tildesley, D. J. *Mol. Phys.* **1997**, *92*, 625.
- (110) Warren, G. L.; Patel, S. *J. Phys. Chem. B* **2008**, *112*, 11679.
- (111) Kirkwood, J. G.; Buff, F. P. *J. Chem. Phys.* **1949**, *17*, 338.
- (112) Chen, B.; Xing, J.; Siepmann, J. I. *J. Phys. Chem. B* **2000**, *104*, 2191.
- (113) Clough, S. A.; Beers, Y.; Klein, G. P.; Rothman, L. S. *J. Chem. Phys.* **1973**, *59*, 2254.
- (114) Murphy, W. F. *J. Chem. Phys.* **1977**, *67*, 5877.
- (115) Odutola, J. A.; Dyke, T. R. *J. Chem. Phys.* **1980**, *72*, 5062.
- (116) *CRC Handbook of Chemistry and Physics*, 77th ed.; Lide, D. R., Ed.; CRC: Boca Raton, FL, 1997.
- (117) Krynicki, K.; Green, C. D.; Sawyer, D. W. *Discuss. Faraday Soc.* **1978**, *66*, 199.
- (118) Buckingham, A. D. *Proc. R. Soc. London Ser. A* **1956**, *238*, 235.
- (119) Watanabe, K.; Klein, M. L. *Chem. Phys.* **1989**, *131*, 157.
- (120) Cini, R.; Logio, G.; Ficalbi, A. *J. Colloid Interface Sci.* **1972**, *41*, 287.